

TimeRadar: A Domain-Rotatable Foundation Model for Time Series Anomaly Detection

Hui He*
huihe@smu.edu.sg
School of Computing and Information Systems
Singapore Management University
Singapore

Hezhe Qiao*
hezheqiao.2022@phdcs.smu.edu.sg
School of Computing and Information Systems
Singapore Management University
Singapore

Yutong Chen
chenyutong@cigit.ac.cn
Chongqing Institute of Green and Intelligent Technology, University of Chinese Academy of Sciences
Chongqing, China

Kun Yi
kunyi.cn@gmail.com
State Information Center
Beijing, China

Guansong Pang[†]
gspang@smu.edu.sg
School of Computing and Information Systems
Singapore Management University
Singapore

Abstract

Current time series foundation models (TSFMs) primarily focus on learning prevalent and regular patterns within a predefined time or frequency domain to enable supervised downstream tasks (*e.g.*, forecasting). Consequently, they are often ineffective for inherently unsupervised downstream tasks—such as time series anomaly detection (TSAD), which aims to identify rare, irregular patterns. This limitation arises because such abnormal patterns can closely resemble the regular patterns when presented in the same time/frequency domain. To address this issue, we introduce **TimeRadar**, an innovative TSFM built in a fractional time–frequency domain to support generalist TSAD across diverse unseen datasets. Our key insight is that rotating a time series into a data-dependent fractional time–frequency representation can adaptively differentiate the normal and abnormal signals across different datasets. To this end, a novel component, namely Fractionally modulated Time-Frequency Reconstruction (**FTFRecon**), is proposed in TimeRadar to leverage a learnable fractional order to rotate the time series to the most pronounced angle between a continuous time and frequency domain for accurate data reconstruction. This provides adaptive data reconstruction in an optimal time–frequency domain for each data input, enabling effective differentiation of the unbounded abnormal patterns from the regular ones across datasets, including unseen datasets. To allow TimeRadar to model local abnormality that is not captured by the global data reconstruction, we further introduce a Contextual Deviation Learning (**CDL**) component to

model the local deviation of the input relative to its contextual time series data in the rotatable domain. Extensive experiments on eight popular TSAD benchmarks demonstrate that TimeRadar consistently outperforms a variety of conventional and TSFM-based competing methods, delivering average gains of 10.5% and 29.4% in AUC-R and AUC-P, respectively. Our code will be available at <https://github.com/mala-lab/TimeRadar>.

Keywords

Time Series, Foundation Model, Anomaly Detection

ACM Reference Format:

Hui He, Hezhe Qiao, Yutong Chen, Kun Yi, and Guansong Pang. 2018. TimeRadar: A Domain-Rotatable Foundation Model for Time Series Anomaly Detection. In *Proceedings of (Conference acronym 'XX)*. ACM, New York, NY, USA, 15 pages. <https://doi.org/XXXXXXXX.XXXXXXX>

1 Introduction

Time series anomaly detection (TSAD), which seeks to identify rare, irregular patterns, is crucial for a wide range of applications, including infrastructure security, intelligent operation and maintenance, and space exploration [6, 9, 28, 29, 61, 69, 70]. Despite recent progress driven by deep learning methods, existing methods typically train a separate model for each dataset, resulting in limited generalization across target datasets and degraded anomaly detection performance in scenarios with scarce training data. Motivated by the success of *foundation models* (FMs) in natural language processing [5], some recent studies [3, 11, 14, 20, 32, 36, 47, 56] have established similar paradigms for time series FMs (TSFMs).

Despite the substantial progress, existing TSFMs primarily focus on learning prevalent and regular patterns to enable supervised downstream tasks [3, 11, 12, 16, 20, 21, 32, 47, 55, 56]. However, this objective is mismatched to those in inherently unsupervised downstream tasks, especially the TSAD task where we are interested in detecting rare abnormal events whose patterns are unbounded and can differ significantly from each other across datasets, *e.g.*, the three different types of anomalies in Fig. 1. Furthermore, these TSFMs are often trained in a predefined time or frequency domain,

*Both authors contributed equally to this research.

[†]Corresponding author: Guansong Pang

Permission to make digital or hard copies of all or part of this work for personal or classroom use is granted without fee provided that copies are not made or distributed for profit or commercial advantage and that copies bear this notice and the full citation on the first page. Copyrights for components of this work owned by others than the author(s) must be honored. Abstracting with credit is permitted. To copy otherwise, or republish, to post on servers or to redistribute to lists, requires prior specific permission and/or a fee. Request permissions from permissions@acm.org.

Conference acronym 'XX, Woodstock, NY

© 2018 Copyright held by the owner/author(s). Publication rights licensed to ACM.

ACM ISBN 978-x-xxxx-xxxx-x/YYYY/MM

<https://doi.org/XXXXXXXX.XXXXXXX>

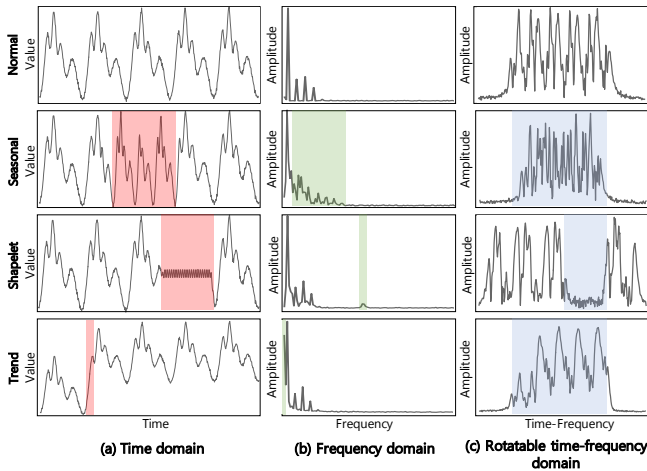


Figure 1: Normal patterns vs. three types of anomaly patterns (trend, shapelet, and seasonal anomalies, highlighted by the colored shadows) across three domains on synthetic data. (a) In the time domain, trend and seasonal anomalies exhibit changes that are highly similar to normal variations, whereas shapelet anomalies are more identifiable. (b) In the frequency domain, shapelet anomalies exhibit changes that are highly similar to normal variations whereas trend and seasonal anomalies produce clearer deviations from the normal patterns. (c) In our proposed rotatable time–frequency domain, all three anomaly types exhibit pronounced deviations from the normal time series.

making them more difficult in detecting these diverse anomalies. This is because certain abnormal patterns can closely mimic normal variations when presented in the same time/frequency domain. For example, as shown in Fig. 1 (a), while shapelet anomalies differ markedly from normal time series, trend and seasonal anomalies induce changes that closely resemble normal temporal variations in the time domain. As a result, time-domain FMs often struggle to localize all these abnormal patterns [3, 11, 12, 14, 27, 32, 46, 47, 56]. A similar issue exists in frequency-domain FMs [20, 54, 55], since frequency domain modeling can weaken the temporal patterns. This is illustrated in Fig. 1 (b), where the shapelet and trend anomalies exhibit only minor differences in the global spectrum.

Very recently there have been some efforts on building FMs specifically for TSAD, such as DADA [46] that is pre-trained to detect anomalies from large-scale multi-domain datasets. However, it is trained in the time domain, suffering from the similar issues as the other time-domain TSADs.

To address these limitations, we introduce **TimeRadar**, an innovative FM built in a rotatable time–frequency domain for enabling generalist TSAD across unseen datasets. The key insight of TimeRadar is that rotating a time series into a data-dependent fractional time–frequency representation can adaptively differentiate the normal and abnormal signals across different datasets. As illustrated in Fig. 1 (c), all three anomaly types exhibit clear and pronounced deviations from the normal time series in a rotatable time–frequency domain (see App. D for more visualizations of anomalies under

different rotation angles). Motivated by this insight, we propose **FTFRecon**, a **F**ractionally modulated **T**ime-**F**requency **R**econstruction component in TimeRadar, in which a learnable fractional order is optimized to rotate time series to the most pronounced angle between the continuous time and frequency domain for minimizing data reconstruction errors. In doing so, FTFRecon can adaptively reconstruct each data input in an optimal time–frequency domain, enabling effective differentiation of the unbounded abnormal patterns from the regular ones across datasets.

To capture local abnormalities that global data reconstruction fails to characterize adequately, we further introduce a Contextual Deviation Learning (**CDL**) component in the rotatable domain, which models the patch-wise deviation of each input with respect to its contextual time series data, promoting compactness among normal samples while enlarging their separation from anomalies with a clear margin. In summary, our contributions are as follows:

- We introduce the TSAD-oriented FM, **TimeRadar**. To the best of our knowledge, TimeRadar is the first TSFM that learns to adaptively detect diverse anomalies across different datasets in a domain-rotatable time–frequency space.
- TimeRadar is instantiated by two novel components, including FTFRecon and CDL. **FTFRecon** is optimized to adaptively identify and rotate the time series to the most pronounced rotation angle in the continuous time–frequency domain, so that the data reconstruction can be performed in the optimal fractional domain for each data input. This helps learn more discriminative TSAD patterns. **CDL** complements the data reconstruction objective in FTFRecon to model local abnormalities by explicitly enforcing large separation between normal and abnormal classes based on the deviation of each input from its contextual time-series.
- Extensive experiments on eight popular TSAD benchmarks demonstrate that TimeRadar delivers the best overall performance, consistently and substantially outperforming both TSFM-based methods and conventional deep TSAD baselines under both zero-shot and few-shot inference settings.

2 Related Work

2.1 Time Series Foundation Models

TSFMs are typically pre-trained on a diverse collection of datasets across multiple domains and can be directly adapted to unseen target domains via zero-shot inference or few-shot fine-tuning [20, 38]. Existing TSFMs can be roughly categorized into those operating purely in the time or frequency domain and those built in the joint time–frequency domain.

TSFMs in the time/frequency domain. TSFMs have been extensively studied under time-domain modeling [3, 14, 27, 32, 46, 47]. The time-domain-based TSFMs can be categorized into encoder-only architectures with masked pre-training objectives [19, 56], decoder-only architectures [11, 42, 47], and encoder-decoder architectures [2, 3, 29]. To capture periodicity changes and energy redistribution patterns, another line of work introduces spectral representations and constructs TSFMs in the frequency domain [8, 58, 66]. Spectral transforms, e.g., Fourier Transform [62, 63], can emphasize characteristic frequency components, making certain anomalies easier to detect. However, in the single time domain

or frequency domain, abnormal patterns can closely resemble the regular patterns, often making the TSFMs ineffective for TSAD.

TSFMs in the time-frequency domain. There are relatively few studies that investigate TSFMs from a time-frequency perspective [13, 52, 58]. They typically fuse time-domain and frequency-domain features into a time–frequency representation and capture how signal energy is distributed across time and frequency. However, these methods rely on a straightforward fusion of time- and frequency-domain features instead of learning a continuous time–frequency representation. In contrast, TimeRadar builds FMs by rotating time series to an input-dependent angle—to better align datasets and capture transferable normal/abnormal patterns to unseen datasets.

2.2 Time Series Anomaly Detection

Most conventional TSAD methods rely on handcrafted statistics or density-based criteria, including one-class classification [59] and neighborhood-based approaches [37]. Recently deep TSAD methods receive much attention, especially in the time domain, which include representation learning based methods [7, 24, 61, 67] and prediction methods [39, 51]. Representation learning methods aim to reconstruct the time series and leverage the reconstruction error as the anomaly score, or leverage the contrastive learning to learn discriminating representations for normal and abnormal time series [10, 24, 61]. Prediction-based methods detect anomalies by learning a forecasting model from historical observations, where anomaly scores are typically computed using the forecasting residual between the predicted value and the observation [31, 45]. Although these deep learning-based models have achieved promising results, they are trained and evaluated on the same dataset, which limits their ability to generalize robustly across diverse TSAD datasets. Recently there have been some studies on TSAD-oriented FMs [27, 38, 46], but they operate in the time domain only, suffering from less discriminative representations on different datasets. In contrast, TimeRadar addresses this issue with a domain-rotatable time-frequency space.

3 The Proposed TimeRadar

3.1 Problem Statement

Time series anomaly detection (TSAD). Given a multivariate time series input $\mathbf{X} = [X_1, X_2, \dots, X_T] \in \mathbb{R}^{T \times C}$ with the number of variates C and the observation length T , the task of TSAD is to output $\hat{\mathbf{Y}} = [y_1, y_2, \dots, y_T] \in \mathbb{R}^{T \times 1}$, where $y_t \in \{0, 1\}$ denotes whether the observation $X_t \in \mathbb{R}^C$ of the t -th time step is anomalous.

Foundation model for Generalist TSAD. This work focuses on developing a foundation model (FM) for enabling generalist TSAD. The model is pre-trained on a collection of I time series datasets from diverse domains, $\mathcal{T}_{\text{train}} = \{\mathcal{D}_{\text{train}}^1, \mathcal{D}_{\text{train}}^2, \dots, \mathcal{D}_{\text{train}}^I\}$, where $\mathcal{D}_{\text{train}}^i = \{\mathbf{X}^i \in \mathbb{R}^{T^{(i)} \times C^{(i)}}, \mathbf{Y}^i \in \mathbb{R}^{T^{(i)} \times 1}\}$ represents the i -th dataset, $C^{(i)}$ and $\mathbb{R}^{T^{(i)}}$ are the number of variates and time points. For downstream evaluation, we consider two settings, including zero- and few-shot anomaly detection. In the few-shot setting, the pre-trained model is further adapted using a small target dataset $\mathcal{D}_{\text{tune}}$, where $|\mathcal{D}_{\text{tune}}| \ll |\mathcal{T}_{\text{train}}|$, and evaluated on an unseen $\mathcal{D}'_{\text{test}}$ from the same domain with $\mathcal{D}'_{\text{tune}}$. In the zero-shot setting, the model is tested directly on $\mathcal{D}'_{\text{test}}$ without any additional adaptation.

Following standard zero- and few-shot settings, $\mathcal{D}'_{\text{tune}}$ and $\mathcal{D}'_{\text{test}}$ are drawn from entirely new domains that are not presented in $\mathcal{T}_{\text{train}}$, i.e., $\mathcal{D}'_{\text{tune}}, \mathcal{D}'_{\text{test}} \not\subseteq \mathcal{T}_{\text{train}}$. Since datasets from diverse domains typically have varying numbers of variates $C^{(i)}$, we apply channel independence [38, 46] to decompose multivariate inputs into univariate series, thus enabling any-variate anomaly detection.

3.2 Overview of the Proposed TimeRadar

As illustrated in Fig. 2, TimeRadar is built upon an encoder-only architecture, which comprises two key components: fractionally modulated time-frequency reconstruction (FTFREcon) and contextual deviation learning (CDL). FTFREcon consists of four steps: fractional domain conversion/inversion, patching & complementary masking, a fractionally modulated encoder, and a reconstruction head. During pre-training, the model is optimized using both a reconstruction loss and a margin-based deviation loss, as detailed in Sec. 3.5. Below we introduce TimeRadar in detail.

3.3 FTFREcon: Fractionally Modulated Time-Frequency Reconstruction

FTFREcon is designed to reconstruct each data input in an optimal fractional time–frequency domain, enabling the learning of normal patterns of the data inputs in a domain-adaptive manner.

Fractional domain conversion/inversion. The Fractional Fourier Transform (FRFT) [65] generalizes the traditional Fourier Transform (FT) [64] by enabling a continuous r -th order counterclockwise rotation in the entire time–frequency plane. This property is particularly advantageous for time series analysis, as FRFT provides a family of intermediate representations that bridge the time and frequency domains. Such representations can well align the dominant time–frequency trajectory of normal signals, while abnormal signals remain misaligned and thus exhibit more dispersed energy distributions, see Fig. 1, which facilitates the discrimination between normal and abnormal patterns in anomaly detection tasks.

Given a univariate time series $X \in \mathbb{R}^T$, we first apply instance normalization [25] and the resulting normalized sequence is then transformed along the temporal dimension using the FRFT to obtain $\mathcal{X}(v_r)$, formulated as:

$$\mathcal{X}(v_r) = \int_{-\infty}^{\infty} K_r(v_0, v_r) X(v_0) dv_0, \quad (1)$$

where v_r denotes the fractional time-frequency variable at the r -th fractional order, v_0 is the integral variable in the time domain, and the kernel function $K_r(v_0, v_r)$ is defined as:

$$K_r(v_0, v_r) = \begin{cases} A_\alpha e^{j\Phi_\alpha(v_0, v_r)}, & \alpha \neq n\pi \\ \delta(v_r - v_0), & \alpha = 2n\pi \\ \delta(v_r + v_0), & \alpha = (2n + 1)\pi \end{cases} \quad (2)$$

where j is the imaginary unit. The FRFT kernel is characterized by the amplitude term $A_\alpha = \sqrt{\frac{1-j \cot \alpha}{2\pi}}$ and the quadratic phase function $\Phi_\alpha(v_0, v_r) = v_0^2 \cot \alpha / 2 - v_r v_0 \csc \alpha + v_r^2 \cot \alpha / 2$. $\delta(\cdot)$ denotes the Dirac delta function, indicating domain identity or domain reversal in the transformation. To capture domain-specific time-frequency characteristics across multi-domain data, we further parameterize the fractional order r as an input-dependent variable learned from

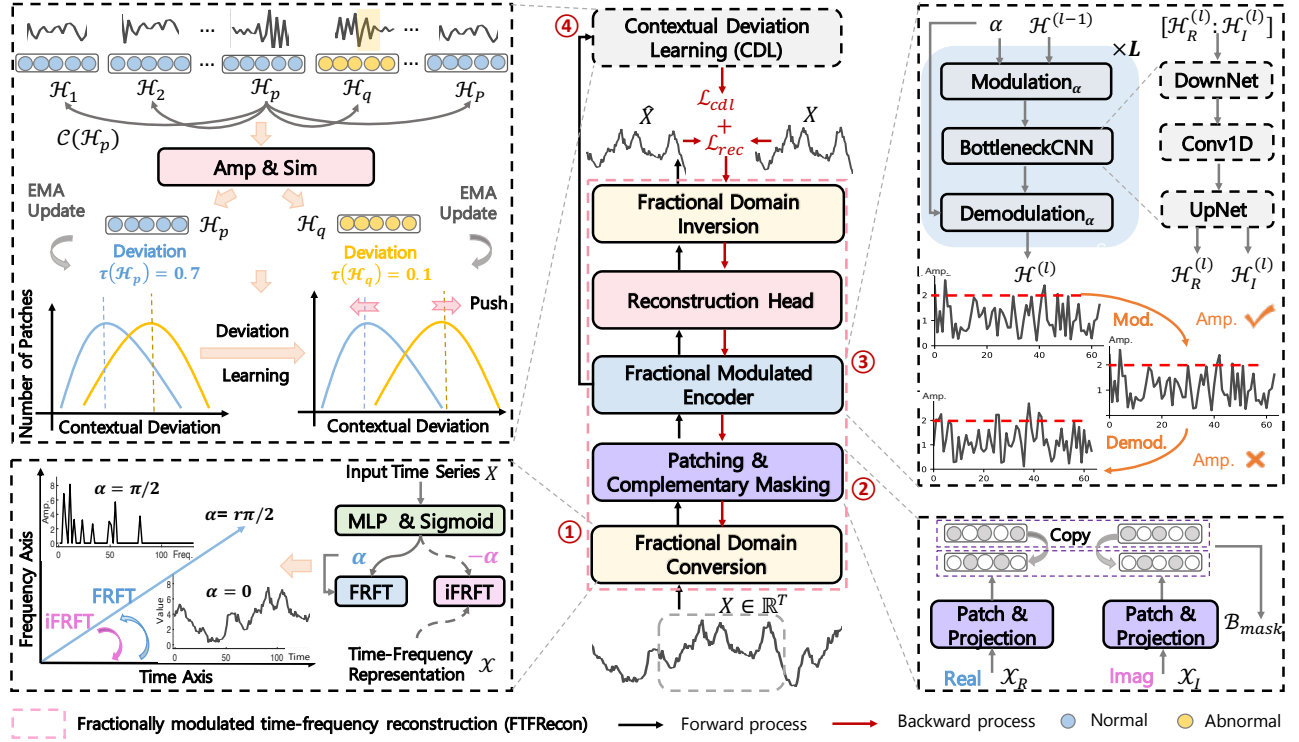


Figure 2: Overview of TimeRadar. Given a time series X , its FTFRecon module firstly ① learns an input-dependent adaptive rotation angle α and accordingly transforms X into a flexible and expressive fractional time–frequency domain. After ② patching and complementary masking, the complex-valued time series patches are fed into the ③ fractionally modulated encoder and a reconstruction head. To complement the data reconstruction with local abnormality modeling, the ④ CDL module models the deviation of each patch relative to its contextual patches in the time–frequency hidden space via a margin learning loss. During pre-training, TimeRadar is jointly optimized with the reconstruction loss \mathcal{L}_{rec} and the margin loss \mathcal{L}_{cdl} .

the input series X , which is then mapped to the rotation angle α , thereby enabling adaptive time–frequency rotation, defined as:

$$\alpha = \frac{r\pi}{2}, r = \text{Sigmoid}(\text{MLP}(X)). \quad (3)$$

After the reconstruction of the masked series in the fractional time–frequency domain, we convert \mathcal{X} back into the time domain using the following inverse conversion formulation:

$$X(v_0) = \int_{-\infty}^{\infty} K_{-r}(v_0, v_r) \mathcal{X}(v_r) dv_r. \quad (4)$$

Patching and complementary masking. Considering that significant amplitude disparities may exist among different components of the input data, the model can be dominated by high-magnitude components, while low-magnitude components are easily suppressed [41, 58, 62]. However, low-magnitude components often capture fine-grained time–frequency deviations that are highly sensitive to abnormal dynamics. Therefore, we introduce a patching and projection step in the fractional domain to extract localized time–frequency patterns. Concretely, given the fractional domain conversion output $\mathcal{X} \in \mathbb{C}^T$, we divide it into P non-overlapping patches of equal length T_p with stride s , where $P = \lceil T - T_p \rceil / s + 1$.

Each patch is then projected into a high-dimensional space of dimension D_p through the projection layer, which is formalized as:

$$\mathcal{B}_R = \text{Projection}(\text{Patch}(\mathcal{X}_R)), \mathcal{B}_I = \text{Projection}(\text{Patch}(\mathcal{X}_I)), \quad (5)$$

where $\text{Projection}(\cdot)$ is implemented by a single linear layer, with \mathcal{X}_R and \mathcal{X}_I denoting the real and imaginary parts of \mathcal{X} , respectively.

To enforce the model see global contextual dependencies, we adopt random patch masking [11, 20, 46] in the fractional time–frequency domain. To preserve phase consistency between the real parts and imaginary parts, this masking is implemented as a shared complementary strategy, where the same patch-wise binary mask and its complement are consistently applied to both parts, yielding dual complementary views of the time–frequency representation. Concretely, \mathcal{B}_R and \mathcal{B}_I can be combined to form the complex-valued representation $\mathcal{B} = \mathcal{B}_R + j\mathcal{B}_I \in \mathbb{C}^{P \times D_p}$. Given the w -th binary mask $\mathcal{M}_w \in \{0, 1\}^P$, two complementary masked representations are then constructed as $\mathcal{M}_w \odot \mathcal{B}$ and $(1 - \mathcal{M}_w) \odot \mathcal{B}$, where \odot denotes element-wise multiplication. The final masked output is obtained by concatenating W complementary mask pairs:

$$\mathcal{B}_{\text{mask}} = \text{Concat}[\mathcal{M}_w \odot \mathcal{B}, (1 - \mathcal{M}_w) \odot \mathcal{B}]_{w=1}^W. \quad (6)$$

Fractionally modulated encoder. An fractionally modulated encoder is designed to model complex-valued time-frequency representations by performing convolution under rotated time-frequency coordinates. Since local phase misalignment may still exist across patches after rotation, modulation is introduced to reduce such inconsistencies and make the representations more compatible with convolutional weight sharing. Given the masked complex-valued representation $\mathcal{B}_{mask} \in \mathbb{C}^{W \times P \times D_p}$, we first apply a stack of fractional modulation blocks, denoted as *FracBlocks*, where each block consists of a modulation-convolution-demodulation procedure in the fractional time-frequency domain. Formally, the fractional modulated learning consists of L *FracBlocks*. For the l -th block, the forward propagation is defined as:

$$\mathcal{H}^{(l)} = \text{Modulation}_\alpha(\mathcal{H}^{(l-1)}), \quad (7)$$

$$\mathcal{H}^{(l)} = \text{BottleneckCNN}(\mathcal{H}^{(l)}), \quad (8)$$

$$\mathcal{H}^{(l)} = \text{Demodulation}_\alpha(\mathcal{H}^{(l)}), \quad (9)$$

where $\mathcal{H}^{(0)} = \mathcal{B}_{mask}$. The modulation operator applies a quadratic-phase chirp to rotate the complex-valued representation, which is implemented by an element-wise multiplication along the P dimension, *i.e.*, $\text{Modulation}_\alpha(\mathcal{H}) = \mathcal{H} \odot_p \mathbf{e}_\alpha$. As shown in Fig. 2, this operation rotates the phase while preserving the amplitude. Correspondingly, the demodulation operator removes the phase rotation by multiplying the complex conjugate chirp, *i.e.*, $\text{Demodulation}_\alpha(\mathcal{H}) = \mathcal{H} \odot_p \mathbf{e}_\alpha^*$, where $(\cdot)^*$ denotes the complex conjugate. The quadratic-phase modulation function is defined as $\mathbf{e}_\alpha = e^{j\pi \cot \alpha \frac{(p-(p-1)/2)^2}{p}}$.

Next, the *BottleneckCNN* in each *FracBlock* is implemented as a real-valued dilated convolution operating on concatenated real and imaginary parts. Since concatenation doubles the representation dimensionality, we introduce a bottleneck into *BottleneckCNN* to control parameterization, which implicitly induces a low-rank structure in the representation space. The computation of *BottleneckCNN* is defined as:

$$\mathbf{H}^{(l)} = \text{DownNet}(\text{Concat}(\mathcal{H}_R^{(l)}, \mathcal{H}_I^{(l)})), \quad (10)$$

$$\mathbf{H}^{(l)} = \text{Conv1D}(\mathbf{H}^{(l)}), \quad (11)$$

$$\mathcal{H}_R^{(l)}, \mathcal{H}_I^{(l)} = \text{Chunk}(\text{UpNet}(\mathbf{H}^{(l)})), \quad (12)$$

where $\text{DownNet}(\cdot)$, $\text{Conv1D}(\cdot)$, and $\text{UpNet}(\cdot)$ are all implemented as 1D convolutions applied along the P dimension, with $\text{DownNet} : \mathbb{R}^{2 * D_p} \rightarrow \mathbb{R}^{D_p}$, $\text{Conv1D}(\cdot) : \mathbb{R}^{D_p} \rightarrow \mathbb{R}^{D_o}$, $\text{UpNet} : \mathbb{R}^{D_o} \rightarrow \mathbb{R}^{2 * D_o}$. Then, we stack $\mathcal{H}_R^{(l)}$ and $\mathcal{H}_I^{(l)}$ to form a complex-valued $\mathcal{H} \in \mathbb{R}^{2 * D_o}$ for the subsequent reconstruction head.

Reconstruction head. Finally, we employ a complex-valued Multi-layer Perception (MLP) [62, 64] to project the modulated time-frequency representation \mathcal{H} into the reconstruction space, formulated as:

$$X = (\text{GeLU}(\mathcal{H}\mathcal{W}_1 + \mathcal{B}_1))\mathcal{W}_2 + \mathcal{B}_2, \quad (13)$$

where \mathcal{W}_1 , \mathcal{W}_2 and \mathcal{B}_1 , \mathcal{B}_2 denote the complex-valued weights and biases, and GeLU is the activation function. The final reconstructed signal $\hat{X} \in \mathbb{R}^{W \times T}$ is obtained by applying inverse FRFT, followed by the amplitude projection:

$$\hat{X} = \text{Amp}(\text{iFRFT}(X)). \quad (14)$$

The reconstruction loss is defined as:

$$\mathcal{L}_{rec} = \frac{1}{T} \sum_{t=1}^T \|X_t - \hat{X}_t\|_2^2. \quad (15)$$

3.4 CDL: Contextual Deviation Learning

Local abnormalities are often overlooked by global reconstruction. To better capture such fine-grained abnormalities that global data reconstruction fails to characterize, we introduce Contextual Deviation Learning (CDL), which enlarges the separation between normal and abnormal patterns in the time–frequency representation, promoting compact normal clusters while pushing anomalies away with a clear margin.

Given the output of the fractional modulated encoder $\mathcal{H} = \{\mathcal{H}_1, \mathcal{H}_2, \dots, \mathcal{H}_p\} \in \mathbb{C}^{W \times P \times D_p}$, the contextual deviation of patch \mathcal{H}_p , denoted as $\tau(\mathcal{H}_p)$, is defined as the aggregated differences to its context patches $\mathcal{C}(\mathcal{H}_p)$ within the same time window of length T :

$$\tau(\mathcal{H}_p) = \frac{1}{P-1} \sum_{\mathcal{H}_q \in \mathcal{C}(\mathcal{H}_p)} (1 - \text{Sim}(\text{Amp}(\mathcal{H}_p), \text{Amp}(\mathcal{H}_q))), \quad (16)$$

where $\text{Sim}(\cdot, \cdot)$ is implemented as the cosine similarity. Then, we adopt a patch-wise margin loss on contextual deviation to explicitly model the contextual deviation difference for normal patches \mathcal{H}_p^N and abnormal patches \mathcal{H}_p^A as follows:

$$\mathcal{L}_{cdl} = \max\{0, \gamma - (\tau(\mathcal{H}_p^N) - \tau(\mathcal{H}_p^A))\}, \quad (17)$$

where $\tau(\mathcal{H}_p^N)$ and $\tau(\mathcal{H}_p^A)$ denote the average contextual deviation of normal and abnormal patches, respectively:

$$\tau(\mathcal{H}^N) = \frac{1}{|\mathcal{H}^N|} \sum_{\mathcal{H}_p \in \mathcal{H}^N} \tau(\mathcal{H}_p), \quad \tau(\mathcal{H}^A) = \frac{1}{|\mathcal{H}^A|} \sum_{\mathcal{H}_p \in \mathcal{H}^A} \tau(\mathcal{H}_p). \quad (18)$$

As illustrated in App. E, by applying CDL, the gap between normal and abnormal patches is larger after training than before, suggesting that CDL strengthens the contextual deviation contrast and yields a more distinct separation between normal and abnormal time series.

3.5 Pre-Training, Fine-Tuning, and Inference

Pre-Training. During pre-training, TimeRadar is optimized under a joint objective consisting of the reconstruction loss and the context-aware margin loss. The reconstruction loss encourages the model to capture normal temporal patterns, such that anomalous samples that deviate from normal behavior yield higher reconstruction errors in the raw space. Meanwhile, the context-aware margin loss further enlarges the separation between normal and abnormal patterns in the representation space. The overall pre-training loss is formulated as:

$$\mathcal{L}_{pretraining} = \mathcal{L}_{rec} + \lambda \mathcal{L}_{cdl}, \quad (19)$$

where λ is a hyperparameter to control the contribution of the CDL module. During optimization, the contextual deviations $\tau(\mathcal{H}_p^N)$ and $\tau(\mathcal{H}_p^A)$ are updated using an Exponential Moving Average (EMA), defined as $\tau^{t+1} = m\tau^t + (1-m)\hat{\tau}^{(t)}$, where m is the EMA momentum and $\hat{\tau}^{(t)}$ is the batch-wise estimate at training step t .

Fine-Tuning. For the fine-tuning under the few-shot setting, we perform head probing [12, 55], where only the reconstruction head is fine-tuned on the target dataset, with the backbone kept frozen.

Inference. During inference, all trainable parameters of TimeRadar are frozen. We compute the reconstruction error together with the variance of multiple reconstructed series at the same time point as the anomaly score $S(X_t)$ [46], defined as:

$$S(X_t) = \text{Var}_W(\hat{X}_t) + \|X_t - \text{Mean}_W(\hat{X}_t)\|_2^2. \quad (20)$$

Anomalous series are typically harder to reconstruct and thus produce more unstable, dispersed reconstructions with higher variance, whereas normal series yield consistent reconstructions with low uncertainty. For performance metrics that require binary outputs, following [46, 58], we apply SPOT [49] to determine the decision threshold, and a point is marked as anomalous if its anomaly score exceeds the threshold.

4 Experiments

4.1 Experimental Setup

Datasets. Leveraging the large-scale publicly available Monash time series repository [17], we curate a diverse multi-domain subset based on the anomalies-injected version released by DADA [46], comprising approximately 408 million time points for pretraining. Following [46, 71], we conduct experiments on 8 popular TSAD datasets to evaluate the effectiveness of TimeRadar, covering a wide range of real-world scenarios including SMD [51], MSL [23], PSM [1], SWaT [35], SMAP [23], CICIDS [26], SWAN [26], and Creditcard [26]. We also evaluate TimeRadar on the UCR benchmark [57], with the results reported in App. B.3. More details about the pretraining and evaluation datasets are provided in App. A.1.

Competing methods. TimeRadar is evaluated against 13 state-of-the-art (SOTA) methods for comprehensive comparison, including (1) *Pretrained TSFMs*: GPT4TS [71], TimesFM [11], Chronos-Bolt [3], Time-MoE [47], SEMPO [20], and DADA [46], where DADA is a generalist model for TSAD; (2) *Conventional TSAD models*: TFMAE [13], Anomaly Transformer [60], DCdetector [61], D3R [53], ModernTCN [34], CATCH [58]. In terms of modeling domains, SEMPO and CATCH operate in the frequency domain, TFMAE in the time-frequency domain, while the remaining models work in the time domain. Detailed descriptions of these baselines are provided in App. A.2. We adopt the default settings for all baselines, including evaluation metrics and thresholding protocols, following common practices in anomaly detection to ensure a fair comparison. Some earlier baseline methods are also considered, with the detailed comparison results provided in App. B.2.

Evaluation metrics. During the evaluation, we deliberately avoid using Point Adjustments (PA) to adjust the detection result, given that some works [22] have demonstrated that PA can lead to faulty performance evaluations. Following the previous work [27, 38], we use the widely-used affiliation-based F1-score (Aff-F1) [22], recently [53, 61], which can take into account the average directed distance between predicted anomalies and ground truth anomalies. We also employed two standard metrics, including AUC-R and AUC-P, which evaluate the detection performance in terms of the area under the ROC curve and the Precision-Recall curve, respectively.

More auxiliary metrics for TSAD evaluation are also reported, with the results provided in App. B.1.

Implementation details. The entire pre-training process takes 3 hours on 2 Pro6000-96G GPUs with BF32 precision and a batch size of 2,048. By default, we set window size $T = 100$, patch size $T_p = 5$, hidden dimension $D_p = 64$, output dimension of Conv1D $D_o = 256$, contextual deviation margin $\gamma = 2$. The weight parameter λ controlling the weight of CDL is set to 0.1. The hyperparameter analysis of T , γ , and λ is given in App. C. Regarding optimization, we employ the AdamW optimizer with hyperparameters: learning rate of 1e-3, weight decay of 0.1, momentum coefficients $\beta_1 = 0.9$ and $\beta_2 = 0.95$. The learning rate is linearly warmed up during the first 10,000 steps and kept constant thereafter.

4.2 Zero-shot Anomaly Detection

As GPT4TS [71] and conventional TSAD models such as Anomaly Transformer [60] are not designed for zero-shot transfer, they are trained separately on the training split of the target dataset and evaluated on its test split, *i.e.*, under the full-shot setting. In contrast, TSFMs follow a zero-shot protocol, being pretrained on multi-domain datasets and directly evaluated on downstream targets without any additional fine-tuning. Table 1 reports the zero-shot performance of FMs and the full-shot performance of conventional TSAD models and GPT4TS.

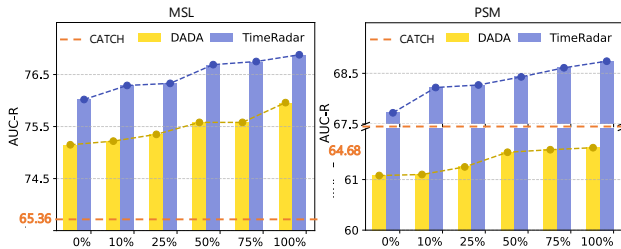
From the results, we have three key observations. (1) TimeRadar consistently surpasses the zero-shot TSAD detector DADA on the majority of datasets, achieving SOTA performance across AUC-R, AUC-P, and Aff-F1. In particular, TimeRadar yields average improvements of 10.5% in AUC-R and 29.4% in AUC-P. This performance gain is largely attributed to the adaptive rotation of the input series into a unified continuous time-frequency domain with a learnable, input-specific angle. Such a transformation effectively exposes anomalies that may remain subtle or indistinguishable in either the pure time or frequency domain, thereby enhancing their saliency and detectability while mitigating cross-domain mismatch. This advantage is further evidenced by the fact that TimeRadar surpasses the pure frequency-domain models CATCH and SEMPO, as well as the time-frequency model TFMAE. (2) FMs such as TimesFM, Chronos-Bolt, Time-MoE, and SEMPO are primarily designed for time series forecasting rather than anomaly detection, and therefore struggle to capture domain-invariant and discriminative normality and abnormality, resulting in inferior cross-domain performance; (3) Generalist TSAD models, *i.e.*, TimeRadar and DADA, surpass conventional TSAD baselines that are trained and evaluated on a single dataset. This strongly suggests that large-scale pretraining on diverse datasets yields far more transferable notions of normality and abnormality, while single-dataset training is inherently limited.

4.3 Few-shot Anomaly Detection

As shown in Fig. 3, following DADA [46], we further fine-tune TimeRadar and DADA on two downstream datasets, MSL and PSM, under varying levels of data scarcity to facilitate domain-specific adaptation. The performance of both models improves as the proportion of available training data increases. Notably, TimeRadar consistently outperforms DADA across all training-data percentages and even surpasses the strongest full-shot baseline, CATCH.

Table 1: Quantitative results for TimeRadar (Ours) in eight real-world datasets. The best ones are in bold, and the second ones are underlined. Avg. denotes the average performance.

Dataset	Setting	Method	SMD	MSL	PSM	SWaT	SMAP	CICIDS	SWAN	Creditcard	Avg.
AUC-R	Full-shot	TFMAE	29.37	45.19	33.35	56.04	58.49	50.41	40.21	47.68	45.09
		Anomaly Transformer	36.74	49.06	49.99	39.69	49.60	51.23	50.86	52.66	47.48
		DCdetector	47.99	50.19	49.44	49.86	49.97	54.48	50.34	44.47	49.59
		D3R	72.01	45.77	58.46	30.01	46.93	61.82	55.63	92.39	57.88
		ModernTCN	70.21	63.04	58.91	24.04	43.42	70.22	52.63	83.54	58.25
		CATCH	73.59	65.36	<u>64.68</u>	23.49	47.26	<u>78.20</u>	49.26	95.41	62.16
		GPT4TS	74.15	58.85	56.26	23.64	48.19	64.27	50.88	95.65	58.99
	Zero-shot	TimesFM	62.80	69.69	51.04	80.98	57.57	58.13	62.07	60.91	62.15
		Chronos-Bolt	63.40	67.14	51.03	80.97	<u>58.56</u>	56.45	62.98	60.85	62.67
		Time-MoE	61.94	61.04	54.68	80.96	42.65	57.05	<u>63.37</u>	58.99	60.08
		SEMPO	57.14	73.46	51.65	47.22	51.97	51.99	46.91	65.27	55.70
		DADA	71.98	75.15	61.08	79.96	51.24	69.24	52.90	95.66	<u>69.15</u>
		TimeRadar	74.54	76.02	67.72	83.31	59.85	82.76	81.13	90.41	<u>76.97</u>
		Avg.									
AUC-P	Full-shot	TFMAE	03.15	09.64	21.54	13.99	<u>15.41</u>	00.09	29.97	00.23	11.75
		Anomaly Transformer	03.87	10.47	28.05	11.71	12.76	00.10	33.71	01.81	12.81
		DCdetector	04.00	11.01	24.79	12.16	12.78	00.11	21.13	00.16	10.77
		D3R	14.18	09.45	38.11	09.45	11.75	00.14	42.28	05.17	16.32
		ModernTCN	14.95	15.20	38.26	09.21	10.96	00.14	45.77	01.65	17.02
		CATCH	<u>16.01</u>	16.34	<u>43.16</u>	08.70	12.14	<u>00.20</u>	42.96	09.08	18.57
		GPT4TS	<u>15.85</u>	13.83	<u>35.82</u>	08.41	12.23	00.12	46.00	08.30	17.57
	Zero-shot	TimesFM	07.37	20.26	29.30	<u>69.32</u>	14.31	00.14	50.24	00.28	23.90
		Chronos-Bolt	07.64	18.72	29.24	69.19	15.25	00.13	49.95	00.32	23.80
		Time-MoE	07.25	16.79	32.31	69.21	11.62	00.14	<u>50.92</u>	00.26	23.56
		SEMPO	06.60	22.04	30.58	10.93	12.55	00.12	31.17	01.74	14.97
		DADA	13.16	26.42	38.79	50.59	12.08	00.14	48.63	<u>09.10</u>	<u>24.86</u>
		TimeRadar	16.09	<u>24.38</u>	44.44	70.33	16.42	00.38	76.02	09.32	32.67
		Avg.									
Aff-F1	Full-shot	TFMAE	63.36	67.04	65.64	68.89	70.72	25.34	09.19	41.90	51.51
		Anomaly Transformer	66.42	66.49	65.37	69.39	71.65	34.70	33.67	62.81	58.81
		DCdetector	66.45	70.56	66.99	69.03	68.99	45.02	24.01	59.65	58.84
		D3R	78.02	77.02	80.29	<u>74.39</u>	74.09	67.79	43.19	70.40	70.65
		ModernTCN	83.16	77.17	79.59	71.13	67.41	51.74	46.45	73.80	68.81
		CATCH	84.46	70.97	79.50	71.82	66.06	72.66	53.37	<u>73.85</u>	71.59
		GPT4TS	83.13	77.23	81.44	70.11	<u>74.67</u>	54.00	47.27	72.88	70.09
	Zero-shot	TimesFM	72.52	74.17	69.58	71.79	72.00	67.45	69.06	68.30	70.61
		Chronos-Bolt	68.34	75.78	69.14	70.98	73.91	67.41	68.82	67.55	70.24
		Time-MoE	72.23	66.05	69.02	69.02	70.87	64.39	62.22	66.43	67.53
		SEMPO	72.35	74.45	73.07	60.31	66.18	34.35	71.25	68.07	64.88
		DADA	<u>84.57</u>	<u>78.27</u>	81.58	73.70	74.13	<u>73.49</u>	71.93	74.84	<u>76.56</u>
		TimeRadar	84.80	79.44	82.03	76.73	75.41	73.51	<u>71.06</u>	72.34	76.92
		Avg.									

**Figure 3: Few-shot performance of TimeRadar and DADA using different amount of training data in a target dataset.**

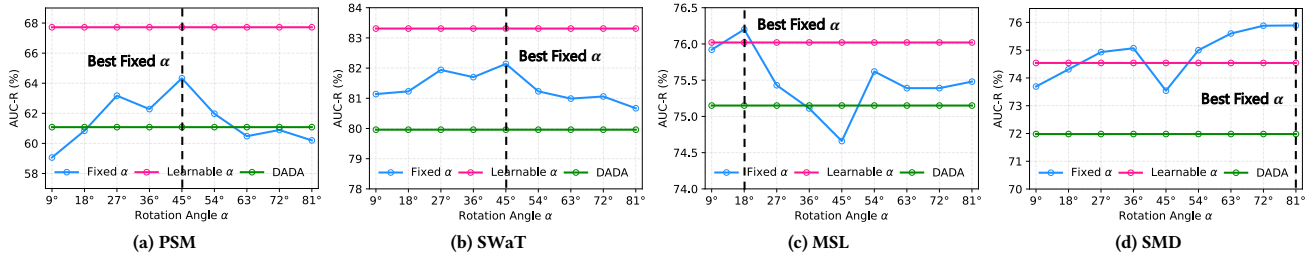
These findings demonstrate the pivotal role of TimeRadar’s pre-trained initialization, which equips the model with strong inductive biases for downstream learning. Consequently, TimeRadar achieves more effective adaptation to domain-specific patterns even in resource-constrained regimes and exhibits a stronger ability to transfer knowledge to previously unseen data.

4.4 Ablation Study

Analysis of key components. To verify the effectiveness of each component in TimeRadar, we designed four variants, including: **A.1 Frequency domain + CDL**, which replaces the FRFT with the FT and employs only the BottleneckCNN within *FracBlocks* as the encoder; **A.2 Time domain + CDL**, which removes the FRFT, adopts the BottleneckCNN as the encoder, and utilizes a real-valued MLP as the reconstruction head; **B BottleneckCNN Encoder**, which uses the BottleneckCNN in *FracBlocks* as the encoder without fractional modulation; and **C TimeRadar (w/o CDL)**, which removes the CDL module during pretraining. The experimental results are summarized in Table 2. We observe that introducing CDL in either the time domain **A.2** or frequency domain **A.1** in isolation yields inferior performance compared with TimeRadar. This underscores the necessity of a unified and continuous time–frequency transformation, which enables learning in a more discriminative and expressive representation space. By adaptively aligning the time–frequency characteristics of normal patterns, TimeRadar better separates normal from abnormal patterns, thereby exposing

Table 2: Ablation study results. The higher values indicate better performance. The best ones are in bold.

Design	MSL			SMAP			SWaT			PSM			CICIDS			SWAN		
	Aff-F1	AUC-R	AUC-P															
TimeRadar	79.44	76.02	24.38	75.41	59.85	16.42	76.73	83.31	70.33	82.03	67.72	44.44	73.51	82.76	00.38	71.06	81.13	76.02
A.1 Frequency domain + CDL	76.69	72.61	22.57	73.74	58.52	15.10	73.46	80.23	69.33	79.20	63.98	38.99	69.48	78.64	00.24	68.37	77.39	72.22
A.2 Time domain + CDL	70.03	73.06	21.49	70.67	51.32	12.31	70.52	82.27	69.72	71.79	65.45	44.29	67.96	73.30	00.20	70.38	79.39	69.04
B BottleneckCNN Encoder	77.66	75.08	23.84	73.27	58.26	14.96	74.63	80.46	69.38	80.12	64.96	40.73	70.12	79.20	00.25	69.41	76.92	72.21
C TimeRadar(w/o CDL)	77.33	75.40	23.86	74.03	58.81	15.73	74.51	80.39	69.60	79.47	62.02	38.72	69.26	80.73	00.27	68.19	78.43	73.74

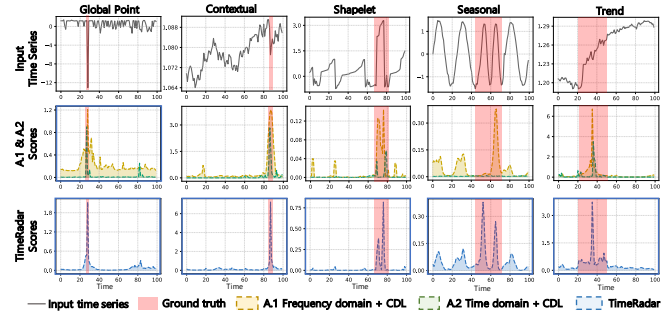
**Figure 4: Comparison of TimeRadar (learnable rotation angle) to its variants with manually searched rotation angles.**

anomalies that may remain subtle or indistinguishable when modeled in a single domain. Furthermore, the variant **C** consistently degrades performance, corroborating the crucial role of CDL in enhancing normal-abnormal separability in the time–frequency representation space by encouraging compact normal clusters and enforcing a clear margin from anomalies. Finally, removing fractional modulation from *FracBlocks*, *i.e.*, the variant **B**, also reduces performance, justifying the importance of local phase alignment across patches in the time–frequency domain, which makes the learned representations more compatible with convolutional weight sharing.

Effectiveness of learnable fractional order. To further demonstrate the effectiveness of TimeRadar with a rotatable domain, we compare it with variants using a wide range of various rotation angles α on four datasets, with a step size of 9° . The results are shown in Fig. 4, with DADA’s performance used as baseline. It is clear that (1) the best rotation angle often differ largely in different datasets and (2) the rotation angle learned by TimeRadar yields highly comparable performance to the best rotation angle found in the grid search across all four datasets, demonstrating that the learned rotation angle in TimeRadar can effectively and adaptively align each dataset to a dataset-specific orientation in the continuous time–frequency space. This offers TimeRadar the strong capability of flexibly adapting to a new dataset based on its data input, supporting its superior generalizability.

4.5 Further Analysis of TimeRadar

Visualization of anomaly scores. To further demonstrate the effectiveness of adaptively transforming the series into an data-dependent continuous time–frequency domain, we conduct a comparative visualization of anomaly scores produced by TimeRadar and its variants, **A.1 Frequency domain + CDL** and **A.2 Time**

**Figure 5: Visualization of anomaly scores.**

domain + CDL, as described in Sec. 4.4. As shown in Fig. 5, we present five representative anomaly types [26] spanning point and subsequence anomalies, where all cases are drawn from real-world datasets except for the seasonal anomaly from synthetic datasets [58]. Successful detection cases are highlighted by blue boxes. From the results, we can observe that for simple point anomalies (first and second columns), global point anomalies are consistently identified by all three methods, whereas the frequency-domain variant **A.1** fails to correctly detect the contextual point anomalies. For more complex subsequence anomalies (third to fifth columns), the variant **A.1** shows strong sensitivity to the true boundaries of shapelet and seasonal anomalies, while the variant **A.2** exhibits either excessively sharp responses (*e.g.*, shapelet and trend anomalies) or overly smooth variations (*e.g.*, seasonal anomalies) around the anomaly regions, leading to unreliable recognition. This observation aligns with the findings in Fig. 1. In contrast, TimeRadar accurately identifies all challenging subsequence anomalies, benefiting from the learnable fractional time–frequency domain.

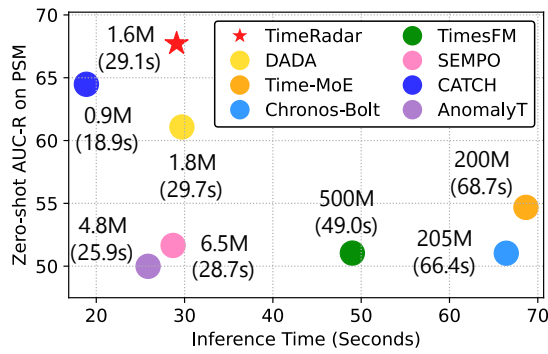


Figure 6: Efficiency comparison on PSM.

Efficiency analysis. We compare the inference costs of TimeRadar with five FMs as well as two conventional anomaly detectors, CATCH and Anomaly Transformer, on the PSM dataset, as shown in Fig.6. All experiments are conducted on a single Pro6000 GPU with a batch size of 128. Compared with existing FMs such as DADA, Chronos-bolt and TimesFM, TimeRadar has faster inference and contains only 1.6M parameters. Although its parameter count and inference time are higher than those of conventional TSAD models, TimeRadar provides a more favorable trade-off between effectiveness and efficiency than both conventional TSAD models and large-scale TSFMs, making it more practical for real-world deployment.

5 Conclusion

In this paper, we introduce a novel FM, TimeRadar, which is the first TSFM that learns to adaptively detect diverse anomalies across different datasets in a domain-rotatable time–frequency space. TimeRadar is implemented with FTFRecon and CDL. FTFRecon enables input-dependent data reconstruction in an optimal time–frequency representation by adaptively rotating each time series to the most pronounced angle between the continuous time and frequency domain. CDL is designed to capture local abnormalities by modeling how an input segment deviates from its surrounding context in the learned fractional time–frequency domain. Extensive experiments show the superiority of TimeRadar over SOTA conventional TSAD and TSFM methods under both zero-shot and few-shot settings.

References

- [1] Ahmed Abdulaal, Zhuanghua Liu, and Tomer Lancewicki. 2021. Practical approach to asynchronous multivariate time series anomaly detection and localization. In *Proceedings of the 27th ACM SIGKDD conference on knowledge discovery & data mining*. 2485–2494.
- [2] Abdul Fatir Ansari, Oleksandr Shchur, Jaris Küken, Andreas Auer, Boran Han, Pedro Mercado, Syama Sundar Rangapuram, Huibin Shen, Lorenzo Stella, Xiyuan Zhang, Mononito Goswami, Shubham Kapoor, Danielle C. Maddix, Pablo Gueron, Tony Hu, Junming Yin, Nick Erickson, Prateek Mutalik Desai, Hao Wang, Huzefa Rangwala, George Karypis, Yuyang Wang, and Michael Bohlke-Schneider. 2025. Chronos-2: From Univariate to Universal Forecasting. *arXiv preprint arXiv:2510.15821* (2025). <https://arxiv.org/abs/2510.15821>
- [3] Abdul Fatir Ansari, Lorenzo Stella, Ali Caner Türkmen, Xiyuan Zhang, Pedro Mercado, Huibin Shen, Oleksandr Shchur, Syama Sundar Rangapuram, Sebastian Pineda-Arango, Shubham Kapoor, Jasper Zschiegner, Danielle C. Maddix, Hao Wang, Michael W. Mahoney, Kari Torkkola, Andrew Gordon Wilson, Michael Bohlke-Schneider, and Bernie Wang. 2024. Chronos: Learning the Language of Time Series. *Trans. Mach. Learn. Res.* 2024 (2024).
- [4] Markus M Breunig, Hans-Peter Kriegel, Raymond T Ng, and Jörg Sander. 2000. LOF: identifying density-based local outliers. In *Proceedings of the 2000 ACM*

- [5] SIGMOD international conference on Management of data. 93–104.
- [5] Tom Brown, Benjamin Mann, Nick Ryder, Melanie Subbiah, Jared D Kaplan, Prafulla Dhariwal, Arvind Neelakantan, Pranav Shyam, Girish Sastry, Amanda Askell, et al. 2020. Language models are few-shot learners. *Advances in neural information processing systems* 33 (2020), 1877–1901.
- [6] Jinyu Cai, Yuan Xie, Glynnis Lim, Yifang Yin, Roger Zimmermann, and See-Kiong Ng. [n. d.]. Self-Perturbed Anomaly-Aware Graph Dynamics for Multivariate Time-Series Anomaly Detection. In *The Thirty-ninth Annual Conference on Neural Information Processing Systems*.
- [7] David Campos, Tung Kieu, Chenjuan Guo, Feiteng Huang, Kai Zheng, Bin Yang, and Christian S Jensen. 2021. Unsupervised time series outlier detection with diversity-driven convolutional ensembles. *Proceedings of the VLDB Endowment* 15, 3 (2021), 611–623.
- [8] Feiyi Chen, Yingying Zhang, Zhen Qin, Lunting Fan, Renhe Jiang, Yuxuan Liang, Qingsong Wen, and Shuiguang Deng. 2024. Learning multi-pattern normalities in the frequency domain for efficient time series anomaly detection. In *2024 IEEE 40th International Conference on Data Engineering (ICDE)*. IEEE, 747–760.
- [9] Yutong Chen, Hongzuo Xu, Guansong Pang, Hezhe Qiao, Yuan Zhou, and Mingsheng Shang. 2024. Self-supervised spatial-temporal normality learning for time series anomaly detection. In *Joint European Conference on Machine Learning and Knowledge Discovery in Databases*. Springer, 145–162.
- [10] Zahra Zamanzadeh Darban, Qizhou Wang, Geoffrey I. Webb, Shirui Pan, Charu C. Aggarwal, and Mahsa Salehi. 2025. GenIAS: Generator for Instantiating Anomalies in time Series. *arXiv:2502.08262* <https://arxiv.org/abs/2502.08262>
- [11] Abhimanyu Das, Weihao Kong, Rajat Sen, and Yichen Zhou. 2024. A decoder-only foundation model for time-series forecasting. In *ICML*. OpenReview.net.
- [12] Vijay Ekambaram, Arindam Jati, Pankaj Dayama, Sumanta Mukherjee, Nam Nguyen, Wesley M. Gifford, Chandra Reddy, and Jayant Kalagnanam. 2024. Tiny Time Mixers (TTMs): Fast Pre-trained Models for Enhanced Zero/Few-Shot Forecasting of Multivariate Time Series. In *NeurIPS*.
- [13] Yuchen Fang, Jiandong Xie, Yan Zhao, Lu Chen, Yunjun Gao, and Kai Zheng. 2024. Temporal-frequency masked autoencoders for time series anomaly detection. In *2024 IEEE 40th International Conference on Data Engineering (ICDE)*. IEEE, 1228–1241.
- [14] Matthew Faw, Rajat Sen, Yichen Zhou, and Abhimanyu Das. 2025. In-Context Fine-Tuning for Time-Series Foundation Models. In *Forty-second International Conference on Machine Learning, ICML 2025, Vancouver, BC, Canada, July 13-19, 2025 (Proceedings of Machine Learning Research, Vol. 267)*, Aarti Singh, Maryam Fazel, Daniel Hsu, Simon Lacoste-Julien, Felix Berkenkamp, Tegan Maharaj, Kiri Wagstaff, and Jerry Zhu (Eds.). PMLR / OpenReview.net. <https://proceedings.mlr.press/v267/faw25b.html>
- [15] Yuye Feng, Wei Zhang, Yao Fu, Weihao Jiang, Jiang Zhu, and Wenqi Ren. 2024. Sensitivityhue: Multivariate time series anomaly detection by enhancing the sensitivity to normal patterns. In *Proceedings of the 30th ACM SIGKDD Conference on knowledge discovery and data mining*. 782–793.
- [16] Shanghua Gao, Teddy Koker, Owen Queen, Tom Hartvigsen, Theodoros Tsiligkaridis, and Marinka Zitnik. 2024. Units: A unified multi-task time series model. *Advances in Neural Information Processing Systems* 37 (2024), 140589–140631.
- [17] Rakshitha Godahewa, Christoph Bergmeir, Geoffrey I Webb, Rob J Hyndman, and Pablo Montero-Manso. 2021. Monash time series forecasting archive. *arXiv preprint arXiv:2105.06643* (2021).
- [18] Markus Goldstein and Andreas Dengel. 2012. Histogram-based outlier score (hbos): A fast unsupervised anomaly detection algorithm. *KI-2012: poster and demo track 1* (2012), 59–63.
- [19] Mononito Goswami, Konrad Szafer, Arjun Choudhry, Yifu Cai, Shuo Li, and Artur Dubrawski. 2024. MOMENT: A Family of Open Time-series Foundation Models. In *ICML*. OpenReview.net.
- [20] Hui He, Kun Yi, Yuanchi Ma, Qi Zhang, Zhendong Niu, and Guansong Pang. 2025. SEMPO: Lightweight Foundation Models for Time Series Forecasting. *arXiv preprint arXiv:2510.19710* (2025).
- [21] Ruijin Hua, Zichuan Liu, Kun Zhang, and Yiyuan Yang. 2026. Diversified Scaling Inference in Time Series Foundation Models. *arXiv preprint arXiv:2601.17376* (2026).
- [22] Alexis Huet, Jose Manuel Navarro, and Dario Rossi. 2022. Local evaluation of time series anomaly detection algorithms. In *Proceedings of the 28th ACM SIGKDD Conference on Knowledge Discovery and Data Mining*. 635–645.
- [23] Kyle Hundman, Valentino Constantinou, Christopher Laporte, Ian Colwell, and Tom Soderstrom. 2018. Detecting spacecraft anomalies using lstm and nonparametric dynamic thresholding. In *Proceedings of the 24th ACM SIGKDD international conference on knowledge discovery & data mining*. 387–395.
- [24] HyunGi Kim, Siwon Kim, Seonwoo Min, and Byunghan Lee. 2023. Contrastive time-series anomaly detection. *IEEE Transactions on Knowledge and Data Engineering* 36, 10 (2023), 5053–5065.
- [25] Taesung Kim, Jinhee Kim, Yunwon Tae, Cheonbok Park, Jang-Ho Choi, and Jaegul Choo. 2022. Reversible Instance Normalization for Accurate Time-Series Forecasting against Distribution Shift. In *ICLR*. OpenReview.net.

- [26] Kwei-Herng Lai, Daochen Zha, Junjie Xu, Yue Zhao, Guanchu Wang, and Xia Hu. 2021. Revisiting time series outlier detection: Definitions and benchmarks. In *Thirty-fifth conference on neural information processing systems datasets and benchmarks track (round 1)*.
- [27] Tian Lan, Hao Duong Le, Jinbo Li, Wenjun He, Meng Wang, Chenghao Liu, and Chen Zhang. 2025. Towards foundation models for zero-shot time series anomaly detection: Leveraging synthetic data and relative context discrepancy. *arXiv preprint arXiv:2509.21190* (2025).
- [28] Yuxin Li, Wenchao Chen, Bo Chen, Dongsheng Wang, Long Tian, and Mingyuan Zhou. 2023. Prototype-oriented unsupervised anomaly detection for multivariate time series. In *International Conference on Machine Learning, ICML 2023, 23-29 July 2023, Honolulu, Hawaii, USA (Proceedings of Machine Learning Research, Vol. 202)*, Andreas Krause, Emma Brunskill, Kyunghyun Cho, Barbara Engelhardt, Sivan Sabato, and Jonathan Scarlett (Eds.). PMLR, 19407–19424. <https://proceedings.mlr.press/v202/li23d.html>
- [29] Yuxuan Liang, Haomin Wen, Yuqi Nie, Yushan Jiang, Ming Jin, Dongjin Song, Shirui Pan, and Qingsong Wen. 2024. Foundation models for time series analysis: A tutorial and survey. In *Proceedings of the 30th ACM SIGKDD conference on knowledge discovery and data mining*. 6555–6565.
- [30] Fei Tony Liu, Kai Ming Ting, and Zhi-Hua Zhou. 2008. Isolation forest. In *2008 eighth IEEE international conference on data mining*. IEEE, 413–422.
- [31] Xinhong Liu, Xiaoliang Li, Yangfan Li, Fengxiao Tang, and Ming Zhao. 2025. RTdetector: Deep Transformer Networks for Time Series Anomaly Detection Based on Reconstruction Trend. In *Proceedings of the Thirty-Fourth International Joint Conference on Artificial Intelligence, IJCAI 2025, Montreal, Canada, August 16-22, 2025*. ijcai.org, 5788–5796. doi:10.24963/IJCAI.2025/644
- [32] Xu Liu, Jincheng Liu, Gerald Woo, Taha Aksu, Yuxuan Liang, Roger Zimmermann, Chenghao Liu, Junnan Li, Silvio Savarese, Caiming Xiong, and Doyen Sahoo. 2025. Moirai-MoE: Empowering Time Series Foundation Models with Sparse Mixture of Experts. In *ICML*. OpenReview.net.
- [33] Yong Liu, Haoran Zhang, Chenyu Li, Xiangdong Huang, Jianmin Wang, and Mingsheng Long. 2024. Timer: Generative Pre-trained Transformers Are Large Time Series Models. In *ICML*. OpenReview.net.
- [34] Donghao Luo and Xue Wang. 2024. ModernTCN: A modern pure convolution structure for general time series analysis. In *The twelfth international conference on learning representations*. 1–43.
- [35] Aditya P Mathur and Nils Ole Tippenhauer. 2016. SWaT: A water treatment testbed for research and training on ICS security. In *2016 international workshop on cyber-physical systems for smart water networks (CySWater)*. IEEE, 31–36.
- [36] Marcel Meyer, Sascha Kaltenpoth, Kevin Zalipski, and Oliver Müller. 2025. Time Series Foundation Models: Benchmarking Challenges and Requirements. *arXiv preprint arXiv:2510.13654* (2025).
- [37] Takaaki Nakamura, Makoto Imamura, Ryan Mercer, and Eamonn Keogh. 2020. Merlin: Parameter-free discovery of arbitrary length anomalies in massive time series archives. In *2020 IEEE international conference on data mining (ICDM)*. IEEE, 1190–1195.
- [38] Yuqi Nie, Nam H. Nguyen, Phanwadee Sinthong, and Jayant Kalagnanam. 2023. A Time Series is Worth 64 Words: Long-term Forecasting with Transformers. In *ICLR*. OpenReview.net.
- [39] Guansong Pang, Chunhua Shen, Longbing Cao, and Anton Van Den Hengel. 2021. Deep learning for anomaly detection: A review. *ACM computing surveys (CSUR)* 54, 2 (2021), 1–38.
- [40] Tomáš Pevný. 2016. Loda: Lightweight on-line detector of anomalies. *Machine Learning* 102, 2 (2016), 275–304.
- [41] Xihao Piao, Zheng Chen, Taichi Murayama, Yasuko Matsubara, and Yasushi Sakurai. 2024. Fredformer: Frequency Debaised Transformer for Time Series Forecasting. In *KDD*. ACM, 2400–2410.
- [42] Kashif Rasul, Arjun Ashok, Andrew Robert Williams, Hena Ghonia, Rishika Bhagwatkar, Arian Khorasani, Mohammad Javad Darvishi Bayazi, George Adamopoulos, Roland Riachi, Nadhir Hassen, et al. 2023. Lag-llama: Towards foundation models for probabilistic time series forecasting. *arXiv preprint arXiv:2310.08278* (2023).
- [43] Mayu Sakurada and Takehisa Yairi. 2014. Anomaly detection using autoencoders with nonlinear dimensionality reduction. In *Proceedings of the MLSDA 2014 2nd workshop on machine learning for sensory data analysis*. 4–11.
- [44] Bernhard Schölkopf, Robert C Williamson, Alex Smola, John Shawe-Taylor, and John Platt. 1999. Support vector method for novelty detection. *Advances in neural information processing systems* 12 (1999).
- [45] Li Shen, Yuning Wei, Yangzhu Wang, and Hongguang Li. 2024. AFMF: Time series anomaly detection framework with modified forecasting. *Knowledge-Based Systems* 296 (2024), 11912.
- [46] Qichao Shentu, Beibu Li, Kai Zhao, Yang Shu, Zhongwen Rao, Lujia Pan, Bin Yang, and Chenjuan Guo. 2025. Towards a General Time Series Anomaly Detector with Adaptive Bottlenecks and Dual Adversarial Decoders. In *ICLR*. OpenReview.net.
- [47] Xiaoming Shi, Shiyu Wang, Yuqi Nie, Dianqi Li, Zhou Ye, Qingsong Wen, and Ming Jin. 2025. Time-MoE: Billion-Scale Time Series Foundation Models with Mixture of Experts. In *ICLR*. OpenReview.net.
- [48] Mei-Ling Shyu, Shu-Ching Chen, Kanoksri Sarinnapakorn, and LiWu Chang. 2003. A novel anomaly detection scheme based on principal component classifier. (2003).
- [49] Alban Siffer, Pierre-Alain Fouque, Alexandre Termier, and Christine Largouët. 2017. Anomaly Detection in Streams with Extreme Value Theory. In *KDD*. ACM, 1067–1075.
- [50] Junho Song, Keonwoo Kim, Jeonglyul Oh, and Sungzoon Cho. 2023. Memto: Memory-guided transformer for multivariate time series anomaly detection. *Advances in Neural Information Processing Systems* 36 (2023), 57947–57963.
- [51] Ya Su, Youjian Zhao, Chenhao Niu, Rong Liu, Wei Sun, and Dan Pei. 2019. Robust anomaly detection for multivariate time series through stochastic recurrent neural network. In *Proceedings of the 25th ACM SIGKDD international conference on knowledge discovery & data mining*. 2828–2837.
- [52] Yuting Sun, Guansong Pang, Guanhua Ye, Tong Chen, Xia Hu, and Hongzhi Yin. 2024. Unraveling the 'Anomaly' in Time Series Anomaly Detection: A Self-supervised Tri-domain Solution. In *40th IEEE International Conference on Data Engineering, ICDE 2024, Utrecht, The Netherlands, May 13-16, 2024*. IEEE, 981–994. doi:10.1109/ICDE60146.2024.00080
- [53] Chengsen Wang, Zirui Zhuang, Qi Qi, Jingyu Wang, Xingyu Wang, Haifeng Sun, and Jianxin Liao. 2023. Drift doesn't matter: Dynamic decomposition with diffusion reconstruction for unstable multivariate time series anomaly detection. *Advances in neural information processing systems* 36 (2023), 10758–10774.
- [54] Shuman Wang, Min Gao, Zongwei Wang, Yibing Bai, Feng Jiang, and Guansong Pang. 2025. FreqLLM: Frequency-Aware Large Language Models for Time Series Forecasting. In *Proceedings of the Thirty-Fourth International Joint Conference on Artificial Intelligence, IJCAI 2025, Montreal, Canada, August 16-22, 2025*. ijcai.org, 3389–3397. doi:10.24963/IJCAI.2025/377
- [55] Yihang Wang, Yuying Qiu, Peng Chen, Kai Zhao, Yang Shu, Zhongwen Rao, Lujia Pan, Bin Yang, and Chenjuan Guo. 2025. Towards a General Time Series Forecasting Model with Unified Representation and Adaptive Transfer. In *ICML (Proceedings of Machine Learning Research, Vol. 267)*. PMLR / OpenReview.net.
- [56] Gerald Woo, Chenghao Liu, Akshat Kumar, Caiming Xiong, Silvio Savarese, and Doyen Sahoo. 2024. Unified Training of Universal Time Series Forecasting Transformers. In *ICML*. OpenReview.net.
- [57] Renjie Wu and Eamonn J Keogh. 2021. Current time series anomaly detection benchmarks are flawed and are creating the illusion of progress. *IEEE transactions on knowledge and data engineering* 35, 3 (2021), 2421–2429.
- [58] Xingjian Wu, Xiangfei Qiu, Zhengyu Li, Yihang Wang, Jilin Hu, Chenjuan Guo, Hui Xiong, and Bin Yang. 2025. CATCH: Channel-Aware Multivariate Time Series Anomaly Detection via Frequency Patching. In *ICLR*. OpenReview.net.
- [59] Hongzuo Xu, Yijie Wang, Songlei Jian, Qing Liao, Yongjun Wang, and Guansong Pang. 2024. Calibrated one-class classification for unsupervised time series anomaly detection. *IEEE Transactions on Knowledge and Data Engineering* 36, 11 (2024), 5723–5736.
- [60] Jiehui Xu, Haixu Wu, Jianmin Wang, and Mingsheng Long. 2022. Anomaly Transformer: Time Series Anomaly Detection with Association Discrepancy. (2022).
- [61] Yiyuan Yang, Chaoli Zhang, Tian Zhou, Qingsong Wen, and Liang Sun. 2023. Dcdetector: Dual attention contrastive representation learning for time series anomaly detection. In *Proceedings of the 29th ACM SIGKDD conference on knowledge discovery and data mining*. 3033–3045.
- [62] Kun Yi, Jingru Fei, Qi Zhang, Hui He, Shufeng Hao, Defu Lian, and Wei Fan. 2024. FilterNet: Harnessing Frequency Filters for Time Series Forecasting. In *NeurIPS*.
- [63] Kun Yi, Qi Zhang, Wei Fan, Longbing Cao, Shoujin Wang, Hui He, Guodong Long, Liang Hu, Qingsong Wen, and Hui Xiong. 2025. A Survey on Deep Learning based Time Series Analysis with Frequency Transformation. In *KDD (2)*. ACM, 6206–6215.
- [64] Kun Yi, Qi Zhang, Wei Fan, Shoujin Wang, Pengyang Wang, Hui He, Ning An, Defu Lian, Longbing Cao, and Zhenqiang Niu. 2023. Frequency-domain MLPs are More Effective Learners in Time Series Forecasting. In *NeurIPS*.
- [65] Hu Yu, Jie Huang, Lingzhi Li, Man Zhou, and Feng Zhao. 2023. Deep Fractional Fourier Transform. In *NeurIPS*.
- [66] Wenxin Zhang, Ding Xu, Guangzhen Yao, Xiaojian Lin, Renxiang Guan, Chengze Du, Renda Han, Xi Xuan, and Cuicui Luo. 2025. Frect: Frequency-augmented convolutional transformer for robust time series anomaly detection. In *International Conference on Intelligent Computing*. Springer, 15–26.
- [67] Yan Zhao, Liwei Deng, Xuanhao Chen, Chenjuan Guo, Bin Yang, Tung Kieu, Feiteng Huang, Torben Bach Pedersen, Kai Zheng, and Christian S Jensen. 2022. A comparative study on unsupervised anomaly detection for time series: Experiments and analysis. *arXiv preprint arXiv:2209.04635* (2022).
- [68] Bin Zhou, Shenghua Liu, Bryan Hooi, Xueqi Cheng, and Jing Ye. 2019. Beatgan: Anomalous rhythm detection using adversarially generated time series. In *IJCAI*, Vol. 2019. 4433–4439.
- [69] Qihang Zhou, Jiming Chen, Haoyu Liu, Shibo He, and Wenchao Meng. 2023. Detecting multivariate time series anomalies with zero known label. In *Proceedings of the AAAI Conference on Artificial Intelligence*, Vol. 37. 4963–4971.

- [70] Quan Zhou, Changhua Pei, Fei Sun, Jing Han, Zhengwei Gao, Haiming Zhang, Gaogang Xie, Dan Pei, and Jianhui Li. 2025. KAN-AD: Time Series Anomaly Detection with Kolmogorov-Arnold Networks. In *Forty-second International Conference on Machine Learning, ICML 2025, Vancouver, BC, Canada, July 13-19, 2025 (Proceedings of Machine Learning Research, Vol. 267)*. Aarti Singh, Maryam Fazel, Daniel Hsu, Simon Lacoste-Julien, Felix Berkenkamp, Tegan Maharaj, Kiri Wagstaff, and Jerry Zhu (Eds.). PMLR / OpenReview.net. <https://proceedings.mlr.press/v267/zhou25u.html>
- [71] Tian Zhou, Peisong Niu, Liang Sun, Rong Jin, et al. 2023. One fits all: Power general time series analysis by pretrained lm. *Advances in neural information processing systems* 36 (2023), 43322–43355.
- [72] Bo Zong, Qi Song, Martin Renqiang Min, Wei Cheng, Cristian Lumezanu, Daeki Cho, and Haifeng Chen. 2018. Deep autoencoding gaussian mixture model for unsupervised anomaly detection. In *International conference on learning representations*.

A Experimental Details

A.1 Datasets

Pretraining datasets. The emergence of large-scale publicly available time series collections, *e.g.*, Anomaly Detection Data [46], Monash+ [46], and TSB-AD [27], have resolved data availability issues for building generalist time series anomaly detection models. These collections contain both normal and abnormal time series spanning diverse domains, reflecting a wide spectrum of real-world applications. In this work, we leverage Monash+ as our pretraining dataset, comprising approximately 408 million time points. The normal time series in Monash+ originates from the Monash Prediction Library [17], whose key properties, including domain, sampling frequency, and sequence length are summarized in Table 3. The abnormal time series is synthesized by injecting anomalies into the Monash normal series. Importantly, none of the downstream evaluation datasets are included in our pretraining data. We then set the pretraining training-validation split to 8:2. In the CDL module, patch-wise labels follow a coarse-grained assignment strategy, where a patch is labeled as anomalous if it contains at least one anomalous time point, and otherwise it is labeled as normal.

Following DADA [46], the anomaly injection procedure is summarized as follows. A subsequence from the original time series and an anomaly type are randomly sampled. If the selected subsequence has not been previously modified, the chosen anomaly is injected into it. This process is repeated until the overall anomaly ratio of the sequence reaches a predefined target level.

Evaluation datasets. For zero- and few-shot anomaly detection, we evaluate TimeRadar and the baselines on a diverse collection of datasets spanning multiple domains, including spacecraft, servers, water treatment, finance, networking, and space weather. The datasets include SMD [51], MSL [23], PSM [1], SWaT [35], SMAP [23], CICIDS [26], SWAN [26], Creditcard [26], as well as the UCR benchmark [57]. The UCR benchmark contains 250 sub-datasets, each consisting of a univariate series with a single anomaly segment. Following previous work [46], only the first continuous dimension is retained for MSL and SMAP [53]. A detailed statistical summary of the datasets is provided in Table 4. The feature dimensions ranges from 1 to 72, sequence lengths vary between 58,317 and 708,405, and anomaly ratios span from 0.17% to 27.8%. Such diversity reflects substantial heterogeneity across datasets and enables a comprehensive evaluation of TimeRadar.

Table 3: Multi-domain time series datasets from the Monash Prediction Library [17].

Dataset	Domain	Frequency	Length
Aus. E.D.	Energy	Half Hourly	1,155,264
Wind	Energy	4 Seconds	7,397,147
Wind Farms	Energy	Minutely	172,178,060
Solar Power	Energy	4 Seconds	7,397,223
Solar	Energy	10 Minutes	7,200,857
London Smart M.	Energy	Half Hourly	166,527,216
Saugeen River F.	Nature	Daily	23,741
Sunspot	Nature	Daily	73,924
Weather	Nature	Daily	43,032,000
KDD Cup 2018	Nature	Daily	2,942,364
US Births	Nature	Daily	7,305
FRED_MD	Economic	Monthly	77,896
Bitcoin	Economic	Daily	75,364
NN5	Economic	Daily	87,801

A.2 Competing Baselines

Full-shot competing baselines. The model is trained separately on the target dataset’s training set and evaluated on its corresponding test set.

- TFMAE [13] is a Temporal-Frequency Masked AutoEncoder that utilizes a contrastive criterion to detect anomalies in time series. It contains two Transformer-based autoencoders that respectively incorporate a window-based temporal masking strategy and an amplitude-based frequency masking strategy to learn knowledge without abnormal bias and reconstruct anomalies using the extracted normal information.
- Anomaly Transformer [60] is a new anomaly-Attention mechanism to compute the association discrepancy, where a min-max strategy is devised to amplify the normal-abnormal distinguishability of the association discrepancy.
- DCdetector [61] is a multi-scale dual attention contrastive representation learning model by utilizing a novel dual attention asymmetric. It is designed to create the permuted environment and pure contrastive loss to learn a permutation-invariant representation with superior discrimination abilities.
- D3R [53] tackles the drift via decomposition and reconstruction. In the decomposition, it utilizes data-time mix-attention to dynamically decompose long-period multivariate time series, overcoming the limitation of the local sliding window. The noise diffusion and directly reconstructing the polluted data are employed to avoid retraining once the bottleneck changes.
- CATCH [58] is a framework based on frequency patching, where a Channel Fusion Module (CFM) is encouraged to iteratively discover appropriate patch-wise channel correlations. It clusters relevant channels while isolating adverse effects from irrelevant channels by optimizing a bi-level multi-objective.
- GPT4TS [71] leverages the pre-trained language model and fine-tunes the input embedding, positional embeddings, layer

Table 4: The datasets used for evaluation, where AR represents the anomaly ratio.

Dataset	Domain	Dimension	Training	Validation	Test(labeled)	AR(%)
MSL	Spacecraft	1	46,653	11,664	73,729	10.5
PSM	Server Machine	25	105,984	26,497	87,841	27.8
SMAP	Spacecraft	1	108,146	27,037	427,617	12.8
SMD	Server Machine	38	566,724	141,681	708,420	4.2
SWaT	Water treatment	31	396,000	99,000	449,919	12.1
Creditcard	Finance	29	113,922	28,481	142,404	0.17
CICIDS	Web	72	68,092	17,023	85,116	1.28
SWAN	Space Weather	38	48,000	12,000	60,000	23.8
UCR	Natural	1	1,790,680	447,670	6,143,541	0.6

Table 5: Comparison between pre-trained FMs on time series.

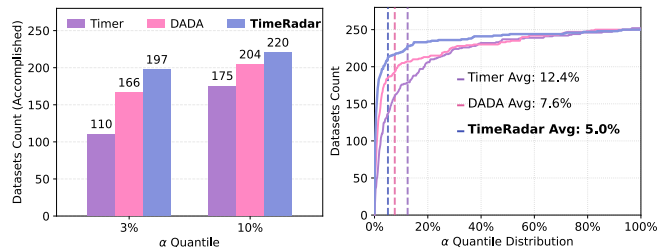
Method	TimeRadar	DADA	SEMPO	Time-MoE	Chronos-Bolt	TimesFM
Architecture	Encoder-only	Encoder-decoder	Encoder-only	Decoder-only	Encoder-decoder	Decoder-only
Model Size	1.6M	1.8M	6.5M	200M	205M	500M
Model version	-	-	Small	Large	Base	v2.0
Input Token	Patch	Patch	Patch	Point	Point	Patch
Dataset Scale	408M	473M	83M	309B	84B	100B
Context Length	100	100	512	≤ 4096	≤ 512	≤ 512
Source	Ours	[46]	[20]	[47]	[3]	[11]

normalization, and output layer to make the pre-trained model adapt to time series data.

- ModernTCN [34] conducts some time series-related modifications to the traditional TCN by using a modern pure convolution structure. It aims to efficiently utilize cross-time and cross-variable dependency for general time series analysis.

Zero-shot competing baselines. The model is trained on multiple source-domain datasets and then directly evaluated on the downstream target-domain test sets without any additional fine-tuning. A comparison between these pre-trained FMs is presented in Table 5.

- TimesFM [11] introduces input patching to represent sequences efficiently, leverages longer output patches to reduce autoregressive steps, and employs random masking to learn from variable-length contexts.
- Chronos-Bolt [3] is proposed for pretrained probabilistic time series models, which tokenize time series values using scaling and quantization into a fixed vocabulary. Existing transformer-based language model architectures are trained on these tokenized time series via the cross-entropy loss.
- Time-MoE [47] introduces a MoE structure into the Transformer framework, enabling sparse activation where only a subset of experts is activated per input token.
- SEMPO [20] is a light generalist time series forecasting model that was built in the frequency domain by modeling both high and low-energy frequency signal.

**Figure 7: Results on UCR benchmark.**

- DADA [46] is the first generalist TSAD that is pre-trained on multiple domains datasets using adaptive bottlenecks and dual adversarial decoders.

B Additional Experiments

B.1 Multi-Metric Results

Because different metrics provide complementary views of model performance and effectiveness, we report three widely used anomaly-detection metrics in the main text: Aff-F1, AUC-R, and AUC-P. To further strengthen the evaluation, we additionally include 6 metrics, with the description provided below and the results summarized in Table 6. TimeRadar still achieves the best performance on all four additional metrics across the three datasets SMD, MSL and PSM, further demonstrating its effective anomaly detection capability.

Table 6: Multi-metrics results in the three real-world datasets. The higher values for all metrics represent better performance. The best ones are in bold, and the second ones are underlined.

Dataset	Method	Aff-P	Aff-R	Aff-F1	AUC-R	AUC-P	R-A-R	R-A-P	V-R	V-P
SMD	Anomaly Transformer	54.08	97.07	66.42	36.74	03.87	51.22	07.09	51.17	07.96
	D3R	64.87	97.93	78.02	72.01	14.18	62.89	11.20	61.69	11.01
	ModernTCN	74.07	94.79	83.16	70.21	14.95	77.54	16.28	77.07	15.96
	GPT4TS	73.33	95.97	83.13	<u>74.15</u>	<u>15.85</u>	<u>77.27</u>	<u>17.68</u>	<u>76.79</u>	<u>17.45</u>
	TimesFM	61.44	88.47	72.52	62.80	07.37	69.72	12.08	74.58	12.69
	Chronos-Bolt	52.69	<u>97.21</u>	68.34	63.40	07.64	70.41	12.45	75.19	13.13
	Time-MoE	60.85	88.84	72.23	61.94	07.25	68.93	11.74	73.82	12.37
	DADA	76.50	94.53	84.57	71.98	13.16	78.14	17.39	77.50	17.13
	TimeRadar	76.60	94.79	84.80	74.54	16.09	78.70	18.32	86.16	24.10
	MSL	Anomaly Transformer	51.04	95.36	66.49	49.06	10.47	50.63	13.07	51.32
D3R		66.85	90.83	77.02	45.77	09.45	56.35	20.05	55.69	19.76
ModernTCN		65.94	93.00	77.17	63.04	15.20	77.88	<u>30.91</u>	77.47	30.10
GPT4TS		64.86	95.43	77.23	58.85	13.83	77.65	28.05	76.97	27.69
TimesFM		59.68	<u>97.95</u>	74.17	69.69	20.26	71.92	24.99	73.94	25.77
Chronos-Bolt		63.91	93.07	75.78	67.14	18.72	71.09	24.35	73.24	25.06
Time-MoE		49.59	98.86	66.05	61.04	16.79	69.48	23.14	71.65	23.62
DADA		68.70	90.56	<u>78.27</u>	<u>75.15</u>	26.42	<u>77.99</u>	31.05	<u>77.48</u>	<u>30.50</u>
TimeRadar		<u>66.88</u>	97.78	79.44	76.02	<u>24.38</u>	79.66	31.05	81.63	35.95
PSM		Anomaly Transformer	54.26	82.18	65.37	49.99	28.05	52.10	33.53	52.86
	D3R	<u>73.32</u>	88.71	80.29	58.46	38.11	52.93	39.62	52.18	39.31
	ModernTCN	73.47	86.83	79.59	58.91	38.26	65.50	<u>47.48</u>	64.80	46.68
	GPT4TS	73.61	91.13	81.44	56.26	35.82	65.16	46.54	64.66	45.99
	TimesFM	53.37	99.99	69.58	51.04	29.30	53.38	34.90	54.56	34.78
	Chronos-Bolt	53.15	<u>98.87</u>	69.14	51.03	29.24	54.67	34.99	54.67	34.99
	Time-MoE	53.91	95.89	69.02	54.68	32.31	60.75	38.52	62.28	38.50
	DADA	73.47	91.71	81.58	61.08	38.79	67.08	47.40	<u>66.52</u>	<u>46.89</u>
	TimeRadar	71.49	96.22	82.03	67.72	44.44	69.62	48.79	72.08	48.00

Table 7: Quantitative results for TimeRadar (Ours) in five real-world datasets. The Aff-P, Aff-R and Aff-F1 represent the Affiliation Precision, Recall and F1 (as %) respectively. The best ones are in bold, and the second ones are underlined.

Dataset	SMD			MSL			SMAP			SWaT			PSM		
	Aff-P	Aff-R	Aff-F1	Aff-P	Aff-R	Aff-F1	Aff-P	Aff-R	Aff-F1	Aff-P	Aff-R	Aff-F1	Aff-P	Aff-R	Aff-F1
OCSVM	66.98	82.03	73.75	50.26	99.86	66.87	41.05	69.37	51.58	56.8	98.72	72.11	57.51	58.11	57.81
PCA	64.92	86.06	74.01	52.69	98.33	68.61	50.62	98.48	66.87	62.32	82.96	71.18	77.44	63.68	69.89
HBOS	60.34	64.11	62.17	59.25	83.32	69.25	41.54	66.17	51.04	54.49	91.35	68.26	78.45	29.82	43.21
LOF	57.69	99.10	72.92	49.89	72.18	29.00	47.92	82.86	60.72	53.20	96.73	68.65	53.90	99.91	70.02
IForest	71.94	94.27	81.61	53.87	94.58	68.65	41.12	68.91	51.51	53.03	99.95	69.30	69.66	88.79	78.07
LODA	66.09	84.37	74.12	57.79	95.65	72.05	51.51	100.00	68.00	56.30	70.34	62.54	62.22	87.38	72.69
AE	69.22	98.48	81.30	55.75	96.66	70.72	39.42	70.31	50.52	54.92	98.20	70.45	60.67	98.24	75.01
DAGMM	63.57	70.83	67.00	54.07	92.11	68.14	50.75	96.38	66.49	59.42	92.36	72.32	68.22	70.50	69.34
LSTM	60.12	84.77	70.35	58.82	14.68	23.49	55.25	27.70	36.90	49.99	82.11	62.15	57.06	95.92	71.55
BeatGAN	74.11	81.64	77.69	55.74	98.94	71.30	54.04	98.30	69.74	61.89	83.46	71.08	58.81	99.08	73.81
Omni	79.09	75.77	77.40	51.23	99.40	67.61	52.74	98.51	68.70	62.76	82.82	71.41	69.20	80.79	74.55
CAE-Ensemble	73.05	83.61	77.97	54.99	93.93	69.37	62.32	64.72	63.50	62.10	82.90	71.01	73.17	73.66	73.42
MEMTO	49.69	98.05	65.96	52.73	97.34	68.40	50.12	99.10	66.57	56.47	98.02	71.66	52.69	83.94	64.74
Anomaly Transformer	54.08	97.07	66.42	51.04	95.36	66.49	56.91	96.69	71.65	53.63	98.27	69.39	54.26	82.18	65.37
DCdetector	50.93	95.57	66.45	55.94	95.53	70.56	53.12	98.37	68.99	53.25	98.12	69.03	54.72	86.36	66.99
SensitiveHUE	60.34	90.13	72.29	55.92	98.95	71.46	53.63	98.37	69.42	58.91	91.71	71.74	56.15	98.75	71.59
D3R	64.87	97.93	78.02	66.85	90.83	77.02	61.76	92.55	74.09	60.14	97.57	74.39	73.32	88.71	80.29
ModernTCN	74.07	94.79	83.16	65.94	93.00	77.17	69.50	65.45	67.41	59.14	89.22	71.13	73.47	86.83	79.59
GPT4TS	73.33	95.97	83.13	64.86	95.43	77.23	63.52	90.56	74.67	56.84	91.46	70.11	73.61	91.13	81.44
TimesFM	61.44	88.47	72.52	59.68	97.95	74.17	58.31	94.10	72.00	61.63	85.95	71.79	53.37	99.99	69.58
Chronos-Bolt	52.69	97.21	68.34	63.91	93.07	75.78	62.24	90.97	73.91	56.19	96.53	70.98	53.15	98.87	69.14
TimeMoE	60.85	88.84	72.23	49.59	98.86	66.05	56.86	94.04	70.87	52.81	99.58	69.02	53.91	95.89	69.02
SEMPO	61.16	88.53	72.35	62.20	92.72	74.45	61.37	71.80	66.18	51.97	71.82	60.31	62.28	88.39	73.07
DADA	76.50	94.53	84.57	68.70	90.56	78.27	66.53	83.69	74.13	59.22	97.54	73.70	73.47	91.71	81.58
TimeRadar	76.60	94.79	84.80	66.88	97.78	79.44	62.90	94.14	75.41	62.23	97.40	76.73	71.49	96.22	82.03

- Aff-P (Affinity-Precision) An affinity-based precision that measures the fraction of predicted abnormal sample affinities

that are truly abnormal (a higher Aff-P indicates fewer false alarms when predicting abnormal affinities).

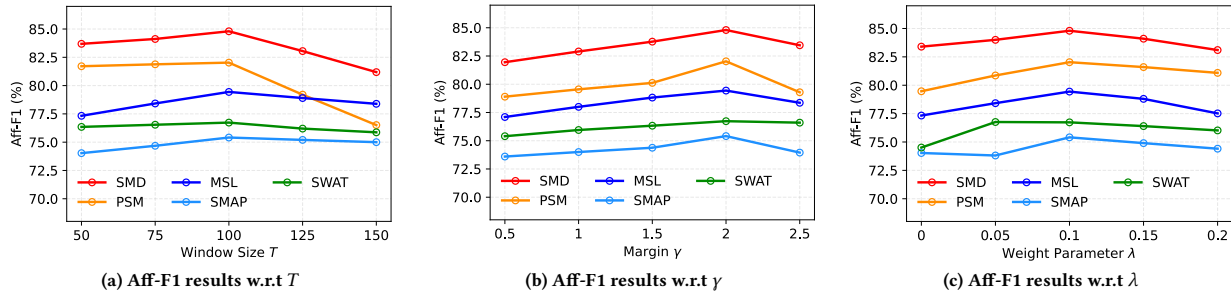


Figure 8: Sensitivity analysis w.r.t window size T , contextual deviation margin γ , and weight parameter λ .

- Aff-R (Affinity-Recall) An affinity-based recall that measures the fraction of truly abnormal samples affinities that are successfully identified as abnormal (a higher Aff-R indicates better coverage of abnormal affinities).
- R-A-R (Range-AUC-ROC): A range-aware ROC AUC that measures detection quality when anomaly samples are contiguous segments, giving credit for overlapping the true anomaly ranges (and being tolerant to small boundary misalignments).
- R-A-P (Range-AUC-PR): A range-aware PR AUC that measures precision–recall performance under segment-based anomaly labeling, rewarding partial/complete coverage of anomaly ranges.
- V-R (VUS-ROC): The Volume Under the ROC, which integrates (range-aware) ROC score over different window sizes, reflecting the robustness to timing misalignment.
- V-P (VUS-PR): The Volume Under the PR, which integrates (range-aware) PR score over different window sizes, capturing robustness across detection tolerances.

B.2 Quantitative Results

Except for several recent strong competing baselines, we also include a set of earlier TSAD baselines for comprehensive comparison. These methods cover: (1) *conventional methods*, including OCSVM [44], PCA [48], HBOS [18], LOF [4], and IForest [30]; and (2) *deep learning methods*, including LODA [40], AE [43], DAGM [72], LSTM [23], CAE-Ensemble [7], SensitiveHUE [15], BeatGAN [68], and MEMTO [50]. The experimental results are reported in Table 7. TimeRadar achieves the best Aff-F1 across all five datasets, consistently outperforming both conventional methods and deep learning baselines. This indicates that TimeRadar attains a more favorable trade-off between precision and recall, making it better suited for real-world practical applications.

B.3 Evaluation on the UCR Benchmark

In this section, following previous studies [46, 57], we evaluate TimeRadar on the UCR Anomaly Archive [57]. The objective is to detect anomalous segments in the test split. For each timestep, anomaly scores are computed and ranked in descending order. If a labeled anomaly interval is detected at a time step with the α quantile, we regard the corresponding anomaly sample as successfully identified by the model. The evaluation results, including: (1)

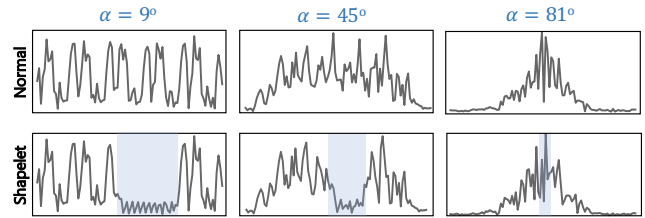


Figure 9: Visualization of the shapelet anomaly in Fig. 1 under the rotatable time–frequency domain with different rotation angles α .

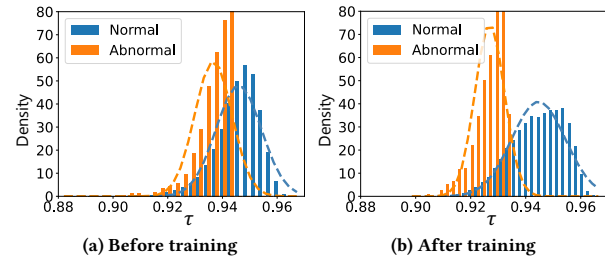


Figure 10: Contextual deviation differences: (a) before training and (b) after training.

the number of successfully detected anomalies at quantile levels of 3% and 10%; and (2) the quantile distribution and the average quantile, are presented in Fig. 7 **left** and **right**, respectively. We observe that under both the 3% and 10% quantiles, TimeRadar detects more anomalous samples than both DADA and Timer [33], indicating its stronger anomaly identification capability and more robust performance across varying quantile levels. As the quantile α increases, TimeRadar, DADA, and Timer identify (*i.e.*, count) more anomaly samples, as expected. Nevertheless, TimeRadar consistently achieves the lowest average quantile compared with DADA and Timer, further indicating its superior effectiveness.

C Sensitive Analysis

The effectiveness of window size T . As shown in Fig. 8 (a), TimeRadar’s performance first improves slightly and then declines as the window size increases. The main reason is that with very short windows, the model sees limited temporal context, while

when the window becomes too long, the abnormal signature becomes less salient in the learned representation. The best results are achieved when the window size is set to 100. Overall, TimeRadar remains stable across a wide range of window sizes, indicating low sensitivity to this hyperparameter.

The effectiveness of contextual deviation margin γ . γ in L_{cdl} denotes the contextual difference we enforce between the normal patch and abnormal patch. As Fig. 8 (b) shows, TimeRadar achieves strong performance on all five datasets across different values of γ , suggesting that enforcing contextual deviation is effective. The best overall results are obtained when $\gamma = 2$. However, γ should not be set too large, since overly strict margins may cause hard anomalies with only subtle contextual deviations to be overlooked. Overall, TimeRadar remains stable under varying margin sizes.

The effectiveness of weight parameter λ . As shown in Figs.8 (c), TimeRadar generally stable as the weight λ varies. The best overall results are obtained when $\lambda = 0.1$. As λ increases, the performance exhibits a slight decline. This is likely excessive emphasis on contextual deviation learning can overly compress the representation space, which in turn reduces the discriminative power of the time–frequency representations.

D More Visualization of Shapelet Anomalies in Rotatable Time–Frequency Domain

We provide the visualization of shapelet anomalies with varying rotation angles, as illustrated in Fig. 9. The discrepancy between anomalous shapelets and normal patterns changes significantly with different rotation angles. When the rotation angle approaches 81° , which can be regarded as a near-frequency-domain setting, the anomalous patterns become less salient. As the angle decreases, the distinction becomes increasingly pronounced, making the anomalies easier to identify.

E Visualization of Contextual Deviation Difference

We visualize the contextual deviation difference before applying CDL and after CDL training to assess its effectiveness, as shown in Fig.10. Applying CDL amplifies the contextual deviation contrast, suggesting that CDL enhances contextual deviation contrast and yields a more distinct boundary between normal and abnormal time series.